Understanding the Effect of Silica Nanoparticles and Exfoliated Graphite Nanoplatelets on the Crystallization Behavior of Isotactic Polypropylene

Diego Pedrazzoli,[1,2] Alessandro Pegoretti,[1] Kyriaki Kalaitzidou[2,3]
[1] *Department of Industrial Engineering and INSTM Research Unit, University of Trento, Trento 38123, Italy*
[2] *G. W. Woodruff School of Mechanical Engineering—Georgia Institute of Technology, Atlanta, GA 30336*
[3] *School of Materials Science and Engineering, Georgia Institute of Technology, Atlanta, GA 30322*

This study explores how the presence of nanofillers with different structural and chemical characteristics, specifically silica nanoparticles and exfoliated graphite nanoplatelets (GNP), alters the crystallization behavior and polymorphism of a semicrystalline polymer, such as polypropylene (PP). The main focus of this research is to investigate how silica and GNP affect the nucleation and growth of PP crystals during isothermal crystallization. The nonisothermal crystallization behavior, including crystal structures, crystallization temperature, and rate, is also determined. PP composites with nanomaterial content up to 7 wt% were produced by melt mixing and injection molding. Both silica and graphite were found to be effective nucleating agents, significantly increasing the crystallization rate during isothermal crystallization, with greater changes observed in case of GNP composites. The effect of filler type and amount on the PP polymorphism and lamella thickness was studied by X-ray diffraction and modulated differential scanning calorimetry. Both silica and graphite were found to be effective nucleating agents for the less common β-phase of PP crystals even at low nanomaterial concentration. α-−crystal perfection and the recrystallization of the β-form in the α-form and/or at the transcrystalline regime were found to be responsible for the recrystallization occurring upon melting in nanocomposites at high silica or medium GNP content. **POLYM. ENG. SCI., 55:672–680, 2015.**

INTRODUCTION

Isotactic polypropylene (PP) can crystallize in various forms or phases. In particular, depending on the crystallization conditions and molecular characteristics, different packing structures of the PP helices lead to the formation of the four well-known crystal forms: monoclinic (α), trigonal (β), triclinic (γ), and smectic (δ) structure [1, 2]. Although the most significant and widely occurring crystal form is the α-form structure, intensive investigation has been recently focused on the β-form because of its interesting physical and mechanical properties [3] including the higher impact strength and toughness of the β-form when compared to the α-form, attributed to the different lamellar morphology of β-PP [4]. Conversely, the Young's modulus and yield strength of isotactic PP, as measured in quasi-static tensile tests, slightly decrease with the β-phase content [5].

As reported [3, 6], the presence of a foreign material (e.g., polymeric compatibilizer, microfiller or nanofiller) can affect the crystallization behavior of semicrystalline polymers including PP. However, only few studies have focused on the effect of foreign materials on the polymorphism of such polymers and the formation of the less common crystalline structure forms [7–9]. It has been shown that the introduction of only 0.5 wt% of *N*, *N*′-dicyclohexylo-2,6-naphthaleno dicarboxy amide as β-phase nucleating agent leads to the formation of almost 100% β-crystalline phase in isotactic PP, with a significant changes of the structure, morphology, and properties [10]. Furthermore, it has been reported that a β nucleating agent, namely calcium pimelate, can be supported on nano-$CaCO_3$ with high specific surface area and significantly increase the efficiency of the β-phase nucleation [11].

The nanofiller itself, in absence of a special nucleating agent, can also promote nucleation of the less common crystalline forms in semicrystalline polymers, for example, as reported [12], clays can promote nucleation of polyamide crystals and induce the formation of the less common β- and γ-form crystals. Other studies investigated the mechanisms responsible for the presence of polymorphism in PP / clay nanocomposites [1, 4, 13]. In particular, the introduction of clay increases the crystallization rate and the crystallization peak temperature, inducing an orientation of the crystals and promoting the formation of the less common β- and γ-phase with a significant enhancement of the impact strength and toughness. In addition to clays, carbon nanotubes [14, 15], and graphite nanoplatelets (GNP) [16], even at low concentration, can also act as nucleating agents for PP. Therefore, the advantage of using nanofillers, especially carbon based ones, over the traditional β nucleating agents is that, in addition to the nucleation of the less common β-phase that exhibits greater toughness and impact strength, there is a dramatic improvement of the mechanical, thermal, and electrical properties achieved at filler content of less than 5 wt% due to the reinforcing effect provided by the rigid inclusions (i.e., higher elastic modulus and yield strength) [17–22]. A thermally conductive polymeric material can be used in various applications such as microchip cooling, fuses, radiators, transformer housings, and so forth. Moreover, a significant reduction of the coefficient of thermal expansion, which is a desirable property for the use of composite structural applications, can be attained. Noteworthy, since the GNP reinforcement are characterized by an aspect ratio greater than 1, a control of the filler's orientation is feasible, in such a way to obtain the desired combination of thermal conductivity and coefficient of thermal expansion.

Although the effects of GNP on the thermal and mechanical properties of various polymers has been widely investigated [23, 24], its influence on the crystallization and melting behavior and polymorphism of semicrystalline polymers still needs to be

Correspondence to: Diego Pedrazzoli; e-mail: pedrazzoli.diego@gmail.com
DOI 10.1002/pen.23941
Published online in Wiley Online Library (wileyonlinelibrary.com).

ascertained. The focus of this research is to determine, by means of modulated differential scanning calorimetry (MDSC), optical microscopy, and X-ray diffraction (XRD), how GNP affects the crystallinity and polymorphism of PP. For the sake of comparison, the effect of conventional filler with different chemical nature and morphology, namely fumed silica nanoparticles, on the crystallization behavior of PP is also investigated.

EXPERIMENTAL SECTION

Materials and Fabrication of *Composites*

The polymer used in this work is an isotactic homopolymer PP (MFI at 190°C and 2.16 kg = 6.9 g/10 min, density = 0.904 g/cm^3) produced by Polychim Industrie S.A.S. (LOON-PLAGE, France) and provided by Lati Industria Termoplastici S.p.A (Varese, Italy) with the commercial code PPH-B-10-FB. The two nanomaterials used are: (i) dimethyldichlorosilane functionalized silica nanoparticles (Aerosil® R974, supplied by Evonik Industries AG—Hanau, Germany) with an average primary particle size of 12 nm and a Brunauer-Emett-Teller (BET) specific surface area of 124 ± 1 m^2/g; and (ii) exfoliated GNPs xGnP-C750, supplied from XG SCIENCE® (East Lansing, MI), with an average diameter of 0.7–0.8 μm and a specific surface area of around 750 m^2/g. Details on the exfoliation process as well as on the morphology of GNP can be found elsewhere [25].

The nanocomposites were produced by melt mixing and injection molding. A vertical, corotating, bench-top twin-screw microextruder (DSM Micro 15 cm^3 Compounder) connected to a microinjection molding unit (DSM) were used to obtain dog-bone specimens. The compound was mixed for 3 min, at 190°C and a screw speed of 250 rpm. The temperature of the mold was 80°C, while the injection molding pressure was about 800 kPa. Composites were designated indicating the matrix and the type of filler with its amount. For instance, a sample filled with 5 wt% of Aerosil® R974 was indicated as PP-silica-5, and the 7 wt% of xGnP-C750 sample was designated as PP-GNP-7.

Experimental Techniques

Morphology Characterization. XRD measurements were obtained on a X'Pert Pro Alpha 1 (PANalytical, Almelo, Netherlands) diffractometer in the Bragg–Brentano geometry, operating at the monochromatic, filtered Cu Kα1 radiation (0.154056 nm). Samples were scanned in a 2θ range between 10° and 50° at a scanning rate of 1°/min, counting time of 4 s, adopting a divergence and antiscatter slit of 1/4° and 1/2°, respectively, at 45 kV and 40 mA. Small square samples 3.3-mm thick, previously washed in acetone and dried using a nitrogen flow, were used for the XRD analyses. Fracture surfaces of samples were observed by a Phenom G2 Pro (Phenom-World BV., Eindhoven, The Netherlands) bench-top scanning electron microscope (SEM), at an acceleration voltage of 5 kV. Prior to the SEM observations, a thin gold coating was applied onto the surface by plasma sputtering to minimize charging effects.

Characterization of the Melting and Crystallization Behavior. Standard and MDSC tests were performed by a DSC Q2000 (TA Instruments, New Castle, DE) under a constant nitrogen flow of 50 ml/min on specimens of about 5–8 mg. Isothermal crystallization studies at 145°C were performed by standard DSC, heating the sample to 200°C at a rate of 30°C/min and maintaining isothermal conditions for 10 min to erase any previous thermal history followed by cooling to 145°C. Every data point is an average of at least three measurements.

The data regarding melting and crystallization behavior was collected by MDSC, heating the samples from the equilibrated temperature of 0°C to 200°C at a rate of 5°C/min, with subsequent cooling to 0°C, at a rate of 5°C/min. During heating and cooling a modulation of ±1°C every 60 s was set to decompose the total heat flow signal into reversing (describing heat capacity events including the glass transition and melting) and nonreversing information (related to kinetic events, such as crystallization and crystal perfection/recrystallization). In particular, the reversing heat flow curves during heating were used to investigate the melting behavior of the nanocomposites. The melting enthalpy (ΔH_m) and melting temperature (T_m) were determined during the heating cycle, whereas crystallization enthalpy (ΔH_c), and crystallization peak temperature (T_c) were determined during the following cooling cycle. In particular, the degree of crystallinity was calculated by taking the weight fraction of PP in the composite into account, according to the following equation:

$$\chi\% = \frac{\Delta H_c}{\Delta H_f^* \left(1 - {}^{wt\%}/_{100}\right)} \times 100 \quad (1)$$

where ΔH_c is the crystallization enthalpy, ΔH_f^* corresponds to the theoretical crystallization enthalpy of 100% crystalline isotactic PP equal to 209 J/g [26], whereas wt% is the filler weight content in percentage.

Isothermal crystallization behavior was also investigated *in situ* using a hot stage (Instec HCS302, Boulder, CO) placed under an optical microscope (Leica DMRM, Buffalo Grove, IL), to heat the samples to 200°C at a rate of 30°C/min. The samples were held isothermally for 10 min and then cooled to the crystallization temperature of 145°C. The temperature was kept constant until the crystallization was completed.

Mechanical Testing. Tensile tests were performed according to ASTM D638 standard with an Instron model 33R 4466 (Norwood) tensile tester equipped with a 500 N load cell. Each data point is an average of at least five tests performed at a crosshead speed of 5 mm/min. Axial strain was recorded using a resistance extensometer Instron® model 2630-101 with a gauge length of 10 mm. To avoid uncertainties related to nonlinearity in the stress-strain curves, elastic modulus was measured as a secant value between longitudinal deformation levels of 0.05% and 0.25%.

The fracture behavior of the material at high strain rate levels was investigated by examining surfaces obtained after impact tests (Izod type) performed according to ASTM D256 standard, by pendulum provided by Custum Scientific Intruments, (Whippany, NJ). The dimensions of the notched Izod impact specimens were $63.5 \times 12.7 \times 3.2$ mm^3, and an edgewise notch of 2.55 mm depth and 0.25 mm radius was made.

RESULTS AND DISCUSSION

Morphological Analysis

The dispersion and distribution of the nanomaterials within the PP matrix were studied using electron microscopy. Fracture

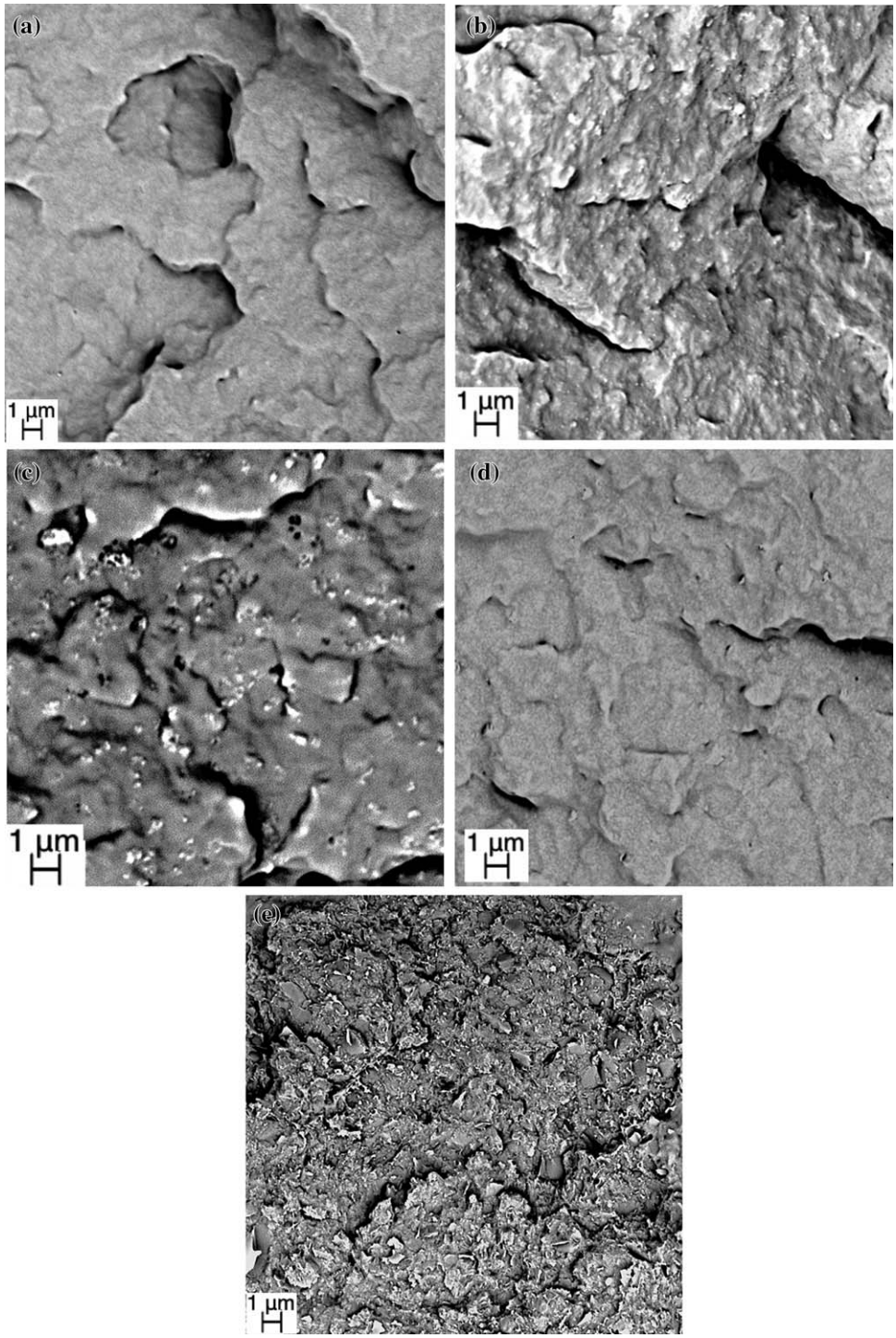

FIG. 1. SEM micropictures of neat PP (a), PP composites filled with 5 and 7 wt% of silica (b, c), and GNP (d, e).

surfaces of PP nanocomposites were analyzed and compared to that of neat PP (Fig. 1a). Although uniform distribution of homogeneous silica aggregates is shown in PP-silica-1 (Fig. 1b), nonhomogeneous agglomeration is evident when considering PP filled with 7 wt% silica (Fig. 1c). GNP appears rather well distributed within the matrix at a content of 1 wt%, with very few distinguishable platelets with dimension of around 1 μm (Fig. 1d). However, larger platelet aggregates can be observed in case of the PP-GNP-7 composites (Fig. 1e). The presence of aggregates may reduce the GNP surface area available for nucleation of the PP crystals.

Isothermal Crystallization Behavior

Representative optical micrographs of the isothermal crystallization studies are reported in Fig. 2. Using the hot stage under the microscope, the temperature is decreased from the melting temperature to 145°C, and then is kept constant until the

 DOI 10.1002/pen

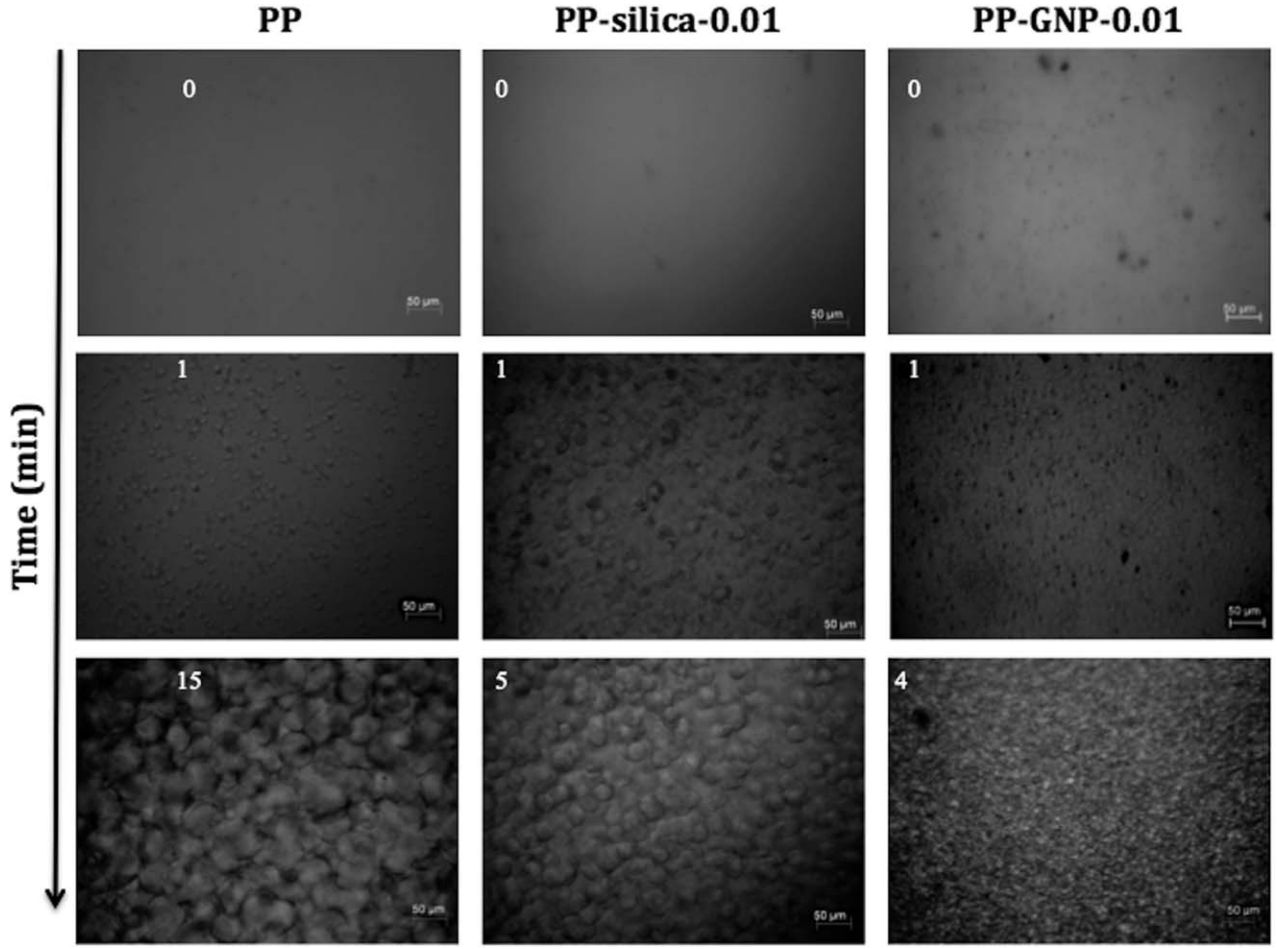

FIG. 2. Hot stage optical pictures during isothermal crystallization at 145°C of PP (left column), PP-silica-0.01 (central column), and PP-GNP-0.01 (right column) as a function of time.

crystallization is completed. In case of neat PP at $t = 0$ (i.e., when the test temperature of 145°C is reached), some pre-existing nuclei can be observed, probably due to impurities and catalyst residues (Fig. 2-left). Crystallization occurs through formation and growth of spherulites around the pre-existing nuclei and no recrystallization or secondary crystallization is observed. Conversely, PP filled with 0.01 wt% silica (Fig. 2-central) or 0.01 wt% GNP (Fig. 2-right) manifests a much faster crystallization which results in smaller spherulites of rather irregular shape compared to those of neat PP, evidencing the nucleation ability of the silica particles and GNP which provide larger surface area available for nucleation and growing of the polymer crystals.

The crystallization rate, a measure of the process kinetics, was determined during isothermal crystallization at 145°C by (i) standard DSC experiments and (ii) *in situ* hot stage/microscopy studies. Results for representative samples are shown in Table 1. It is noted that in case of the *in situ* study the crystallization rate is considered as the inverse of the time required for the spherulites to completely cover the observed micrograph area. In the case of DSC experiments, the crystallization rate was determined as the inverse of the time interval required for the completion of the crystallization during isothermal crystallization. As shown, the two methods resulted in similar values for the crystallization rate clearly indicating that addition of nanomaterials even at the very low content of 0.01 wt% can significantly alter the crystallization characteristics of PP including a dramatic increase of the crystallization rate.

Nonisothermal Crystallization Behavior

The degree of crystallinity ($\chi_{\%}$), determined by MDSC during nonisothermal crystallization, decreases with the filler content (Table 2). The nucleation effect of the nanomaterials is evidenced by an increase in crystallization temperature (T_c) and as shown the nucleating effect of GNP is significantly larger compared to that of silica. The nanomaterials nucleating action is mainly attributed to their high surface area which is 124 and

TABLE 1. Crystallization rate during isothermal crystallization at 145°C based on DSC and *in situ* hot stage/microscopy studies.

Sample	Based on DSC (min^{-1})	Based on *in situ* hot stage/microscopy (min^{-1})
PP	0.069 ± 0.002	0.05
PP-silica-0.01	0.209 ± 0.012	0.20
PP-GNP-0.01	0.331 ± 0.015	0.25

TABLE 2. Crystallization and melting parameters obtained by MDSC.

Sample	T_c (°C)[a]	$\chi_{\%}$ (%)[b] [ΔH_c (J/g)]	Induction time (min)	T_{m1} (°C)[c]	T_{m2} (°C)[d]	Enthalpy of recrystallization (J/g)
PP	126.2 ± 0.2	51.1 ± 0.3 (106.8)	3.7 ± 0.1	154.6 ± 0.1	166.3 ± 0.2	~0
PP-silica-0.5	126.9 ± 0.2	50.6 ± 0.4 (105.2)	3.7 ± 0.1	154.7 ± 0.2	167.6 ± 0.4	~0
PP-silica-1	127.2 ± 0.2	49.8 ± 0.4 (103.1)	3.8 ± 0.0	154.9 ± 0.2	168.0 ± 0.2	~0
PP-silica-3	127.5 ± 0.1	49.7 ± 0.4 (100.8)	4.0 ± 0.1	154.4 ± 0.1	168.6 ± 0.3	~0
PP-silica-5	127.6 ± 0.2	48.3 ± 0.4 (95.9)	4.1 ± 0.1	156.5 ± 0.3	167.1 ± 0.2	2.1 ± 0.2
PP-silica-7	127.7 ± 0.1	47.1 ± 0.3 (91.5)	4.2 ± 0.1	158.6 ± 0.2	167.0 ± 0.4	15.9 ± 0.6
PP-GNP-0.5	130.8 ± 0.2	49.8 ± 0.5 (103.5)	4.2 ± 0.0	/	160.2 ± 0.2	~ 0
PP-GNP-1	133.2 ± 0.2	48.6 ± 0.4 (100.5)	4.7 ± 0.2	/	160.3 ± 0.3	2.5 ± 0.2
PP-GNP-3	137.2 ± 0.2	48.7 ± 0.5 (98.7)	5.0 ± 0.1	/	161.3 ± 0.2	30.9 ± 0.4
PP-GNP-5	138.8 ± 0.2	47.4 ± 0.4 (94.1)	5.2 ± 0.1	/	162.1 ± 0.3	23.5 ± 0.6
PP-GNP-7	139.3 ± 0.3	46.7 ± 0.4 (90.7)	5.5 ± 0.2	/	161.7 ± 0.2	12.2 ± 0.4

[a]Crystallization peak temperature recorded by MDSC.
[b]Degree of crystallinity (crystallization enthalpy in brackets).
[c]First melting peak temperature, recorded on the reversing heat flow curve.
[d]Second melting peak temperature, recorded on the reversing heat flow curve.

750 m^2/g for silica and GNP, respectively, according to the suppliers.

The crystallization induction time, defined as the time difference between onset and endset of nonisothermal crystallization, is increased with the filler content indicating that the polymer chains have more time, at higher temperature, to rearrange forming thus more perfect and/or thicker crystals [27].

In conclusion, addition of nanomaterials in PP results in increase of the crystallization temperature and decrease in the degree of crystallinity, with GNP having a larger effect on these crystallization characteristics compared to silica.

Polymorphism and Crystal Thickness

The effect of filler type and amount on the PP polymorphism and lamella thickness was studied by XRD and MDSC. Isotactic PP can exhibit four crystal structures: monoclinic (α), trigonal (β), triclinic (γ), and smectic (δ), whose formation depends on the melting history, crystallization temperature, pressure, and cooling rate, and the presence of nucleating agents or fillers [2, 28]. In particular, α-form is the most common crystalline phase, while β-−form more likely occurs under particular conditions in terms of temperature gradients, presence of shearing forces [29, 30], or nucleating agents, whereas the γ-form is the least common and is more likely to be observed in low molecular weight PP [31]. Previous studies on the crystallization of isotactic PP demonstrated that a higher amount of the β-form results in higher impact strength and toughness compared to the α-form [16], accompanied with a slight decrease in elastic modulus and yield stress [5].

The diffractograms of PP-silica and PP-GNP nanocomposites are presented in Fig. 3a and b, respectively. The characteristic six reflections of the α-form ($2\theta = 14.08°$ <110>, $2\theta = 16.95°$ <040>, $2\theta = 18.50°$ <130>, $2\theta = 21.85°$ <041>, $2\theta = 25.00°$ <060>, and $2\theta = 28.00°$ <220>) [31–33], two reflections of the β-form ($2\theta = 16.00°$ <300> and $2\theta = 21.00°$ <301>) [32] and one reflection attributable to the γ-form ($2\theta = 20.07°$ <117>) [31] can be recognized on the diffractogram of neat PP (Fig. 3a).

Silica incorporation results in an increase of the first three reflections of the α-form, with the reflection at $2\theta = 16.95°$ dominating, whereas the reflection at $2\theta = 21.85°$ decreases in intensity with the filler amount. Conversely, the β-form reflections increase up to filler content of 0.5 wt% and diminish at higher filler content, whereas the γ reflection (recognizable at $2\theta = 20.07°$) becomes slightly broader with the filler content. Furthermore, it can be seen that addition of 0.01 wt% silica promotes the formation of the β-phase crystals. As confirmed by XRD the silica nanoparticles are amorphous.

The β-phase content, known as k value, was estimated adopting the formula proposed by Turner–Jones et al. [34]:

$$k = \frac{I_\beta}{I_{\alpha1} + I_{\alpha2} + I_{\alpha3} + I_\beta} \times 100[\%] \quad (2)$$

where I_β is the intensity of the β-phase reflection corresponding to the <300> plane, while $I_{\alpha1}$, $I_{\alpha2}$, and $I_{\alpha3}$ are the intensities of the α-phase reflections corresponding to the <110>, <040>, and <130> plane, respectively. An increase, in the order of ~13%, in the k value with silica content up to 0.5 wt% silica can be observed followed by a slow decrease at larger filler contents (Fig. 4a). The nonmonotonical trend of k as a function of the silica content indicates the presence of an optimum silica content which promotes the formation of the less common β-phase. Further addition of silica compromises the available surface of the silica nanoparticles, due to agglomeration, and increases the crystallization rate hindering the formation of β-phase in favor of the α-phase. In particular, β-nuclei have less time to form and insufficient space to grow due to the faster nucleation and growing of the α-nuclei, as confirmed by the estimation of the lamella thickness reported below.

The lamella thickness of the crystals (L_t), which is a measure of the crystal size was calculated using the full width at half maximum of the predominant XRD reflections according to the Debye-Scherrer formula [35], presented in *Eq. 3*

$$L_t = \frac{K \cdot \lambda}{\mathrm{FWHM} \cdot \cos(\theta)} \quad (3)$$

where K is the crystal shape factor assumed as 0.9, while λ is the X-ray source wavelength.

DOI 10.1002/pen

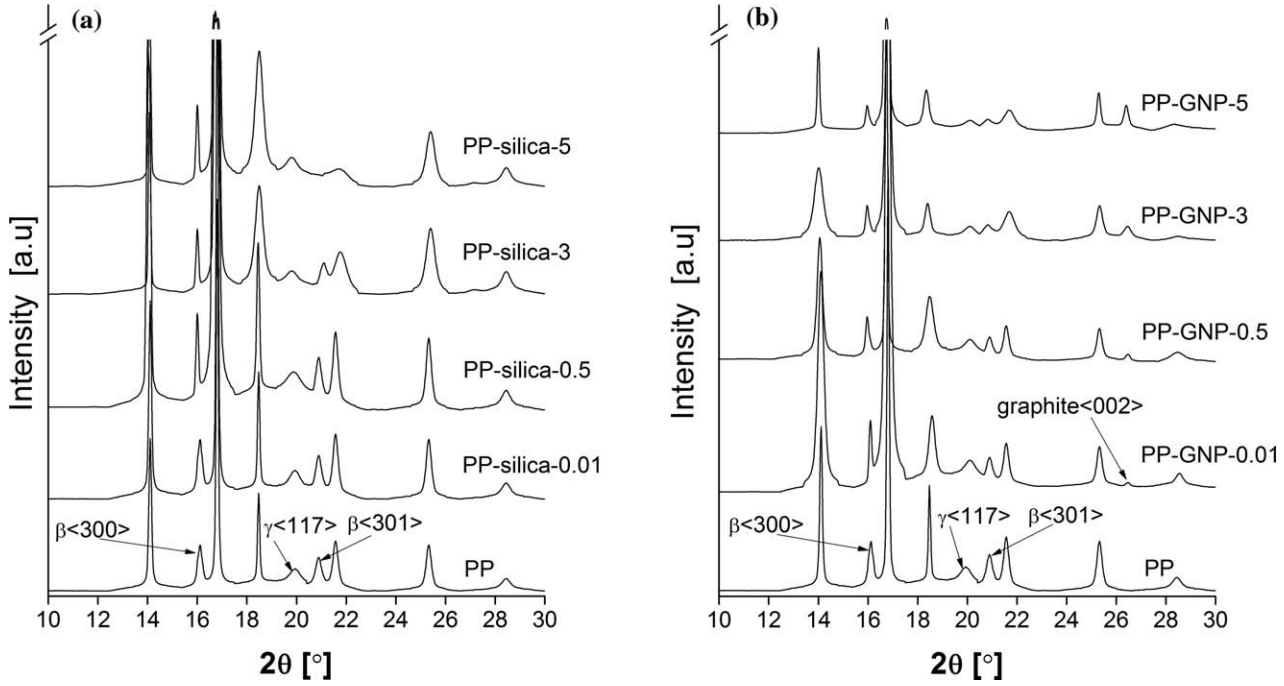

FIG. 3. X-ray diffractograms of (a) PP-silica and (b) PP-GNP nanocomposites as a function of the nanomaterial content.

The thickness of the dominant α-−form crystal of PP-silica composites, corresponding to the reflection at $2\theta = 16.95°$, is found to significantly increase with the silica content (Fig. 4a). Since the α-−form is the predominant crystalline morphology in PP, the higher crystal thickness is in agreement with the increase of induction time as measured during nonisothermal crystallization experiments (Table 2). Conversely, the thickness of the β-−phase crystals ($2\theta = 16.10°$) increases for addition of silica up to 1 wt% and slowly decreases at higher contents, parallel with the reduction in β-phase content.

Incorporation of GNP into PP results in an increase of the reflections of the α-form crystals with the filler content and a slight increase of the reflections associated to the β-form crystals at low GNP content of 0.01 wt%. The β-form reflections are attenuated at higher GNP loadings as shown in Fig. 3b. The presence of nanofiller can be recognized by the reflection at $2\theta = 26.45°$, corresponding to the graphite's <002> plane [36], whose intensity increases with the filler content. It is noted that the graphite reflection in case of the PP-GNP composites does not shift to smaller values of theta compared to the peak of neat GNP,

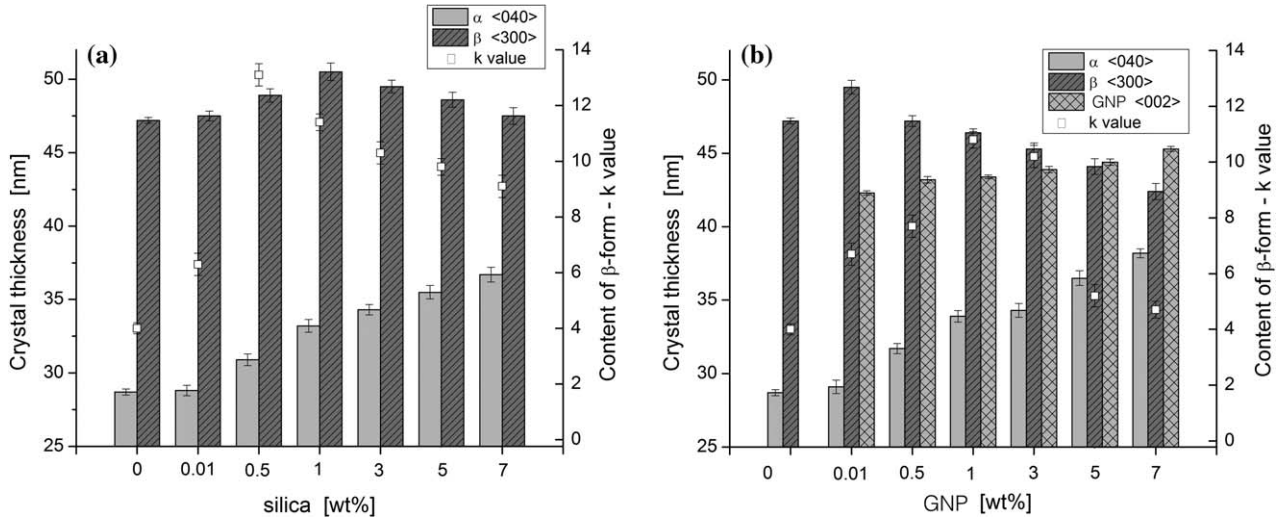

FIG. 4. (a) Crystal thickness of the α-form evaluated at $2\theta = 16.95°$ (<040> plane) and β-form evaluated at $2\theta = 16.00°$ (<300> plane) for PP-silica composites and (b) crystal thickness of the α-form, β-form and of the graphite's <002> plane at $2\theta = 26.45°$.

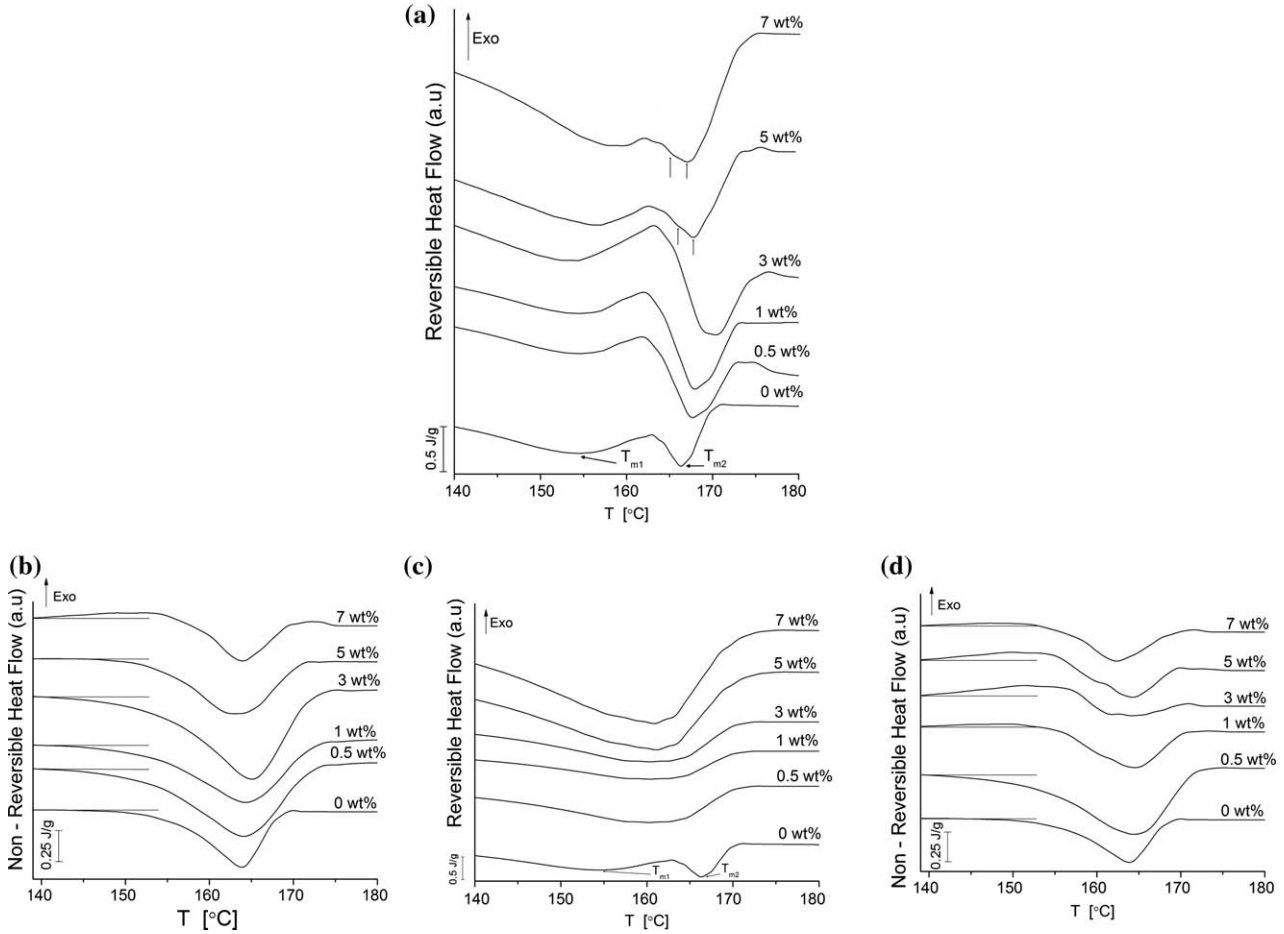

FIG. 5. Reversible and nonreversible heat flow describing the melting behavior of (a, b) PP-silica and (c, d) PP-GNP nanocomposites during MDSC analyses.

indicating that the high viscosity PP melt cannot intercalate the GNP, that is the polymer chains cannot enter into the GNP narrow galleries, as reported also elsewhere [37–39]. Conversely, the crystal size associated to the graphite's <002> plane increases with the filler loading (Fig. 4b), indicating the presence of large oriented agglomerates formed during processing due to poor dispersion and alignment along the injection molding direction [40].

The β-phase content increases up to around 11% corresponding to a graphite content of 1 wt%, as indicated by the k value. However, the higher crystallization rate reached at greater filler amount might favor the formation of the α-phase over the β-phase, inducing a decrease in content and lamellar thickness of the β-phase.

The predominant α-−form crystals manifest a nonmonotonical increase in crystal thickness with filler content, characterized by a plateau between 1 and 3 wt%. The elastic modulus exhibits a similar trend, as shown in Fig. 6. It is understood that the α-−form crystals increase in thickness and reach a plateau when the β-phase content is maximum, followed by a second increase occurring upon a rapid decrease in β-phase content upon further addition of GNP.

Melting Behavior

The results of the structural morphology obtained by XRD are in agreement with the melting behavior as determined using MDSC. In particular, the reversing heat flow measured by MDSC is strictly associated to reversible transformations, including melting related phenomena. PP-silica composites show two distinct peaks on the curve, a minor peak T_{m1} at lower temperature and the main peak T_{m2} at higher temperature (Fig. 5a). The double melting peak might be associated with the recrystallization of the monoclinic α_1 phase into the more ordered α_2 phase [41]. However, as it was shown in XRD diffractograms, PP-silica nanocomposites present a significant β-phase content, whose melting properties differ from those of the α-phase. In fact, the β-phase of isotactic PP manifests a melting peak at lower temperature (i.e., located between 153 and 159°C) compared to the α-phase [10, 42]. Therefore, the two melting peaks T_{m1} and T_{m2} are associated to the β and α crystal form, respectively. Splitting of the low temperature peak T_{m1} is not observed, indicating the absence of a β-β' recrystallization (i.e., due to crystal perfection phenomena of the β-phase), as it might occur in some cases under different cooling condition [43, 44]. Moreover, the melting peak T_{m1} is shifted toward higher temperatures and decreases in intensity at higher filler content, probably because of the β-phase attenuation. Noteworthy, the reversing heat flow excludes all phenomena related to recrystallization and crystal perfection, possibly occurring upon heating. To further investigate the melting behavior, the curve of the nonreversing heat flow was analyzed (Fig. 5b) as a function of the filler content. Limited recrystallization occurs

 DOI 10.1002/pen

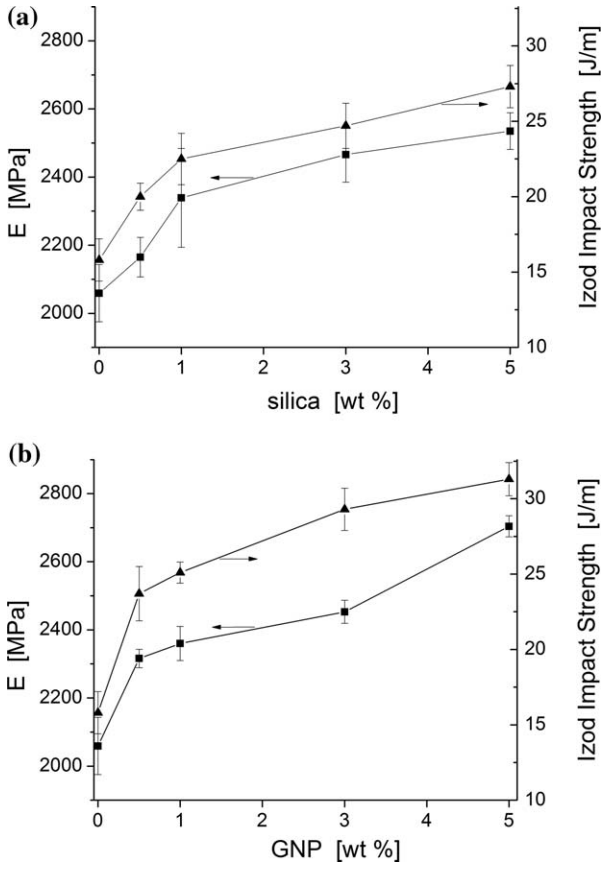

FIG. 6. Elastic modulus and tensile energy at break of (a) PP-silica and (b) PP-GNP nanocomposites.

only at 7 wt% silica, probably because of α- crystals perfection phenomena or because the imperfect β-crystals recrystallize in the α-form and/or at the transcrystalline regime [45–47]. The β–α transition was quantified by computing the recrystallization enthalpy, estimated as the area under the exothermic transformation (Table 2). In general, the more imperfect the trigonal crystals are (i.e., at higher cooling rates), the more intense the β–α transition becomes [42].

As reported in [42], isotactic PP exhibits recrystallization showing a slight but significant splitting of the endotherm peak associated with the α_1 and α_2 phases at 165 and 168°C, respectively, which is also observed on the reversible curves (Fig. 5a) of PP-silica 7 wt%. The new monoclinic crystals that form during the β–α transition are α_2 and melt at a higher temperature than the α_1 crystals, formed during cooling from the melt.

Curves of PP-GNP composites show that the melting peak T_{m1} progressively disappears upon addition of GNP, because the β-phase is hindered (Fig. 5c). Since the two melting peaks T_{m1} and T_{m2} were rather difficult to be distinguished on the curve, only one representative melting temperature was reported in Table 2.

Moreover, recrystallization occurs at filler loadings between 1 and 5 wt%, possibly indicating crystal perfection phenomena or recrystallization of the β-form in the α-form and/or at the transcrystalline zone (Fig. 5d). As confirmed by XRD analysis, the β-form crystals become fewer and thinner with GNP loading larger than 1 wt%, when recrystallization begins to occur.

Therefore, when considering the crystallization induction time based on DSC, the vanishing of the β-phase and the recrystallization enthalpy according to MDSC; and the increased lamella thickness of the α-phase calculated based on XRD, the overall effect of GNP on the crystallization of PP is the formation of more perfect α-crystals.

Tensile and Impact Mechanical Properties

The elastic modulus of the PP-silica and PP-GNP composites increases nonmonotonically with addition of fillers as shown in Fig. 6a and b, respectively. This trend indicates the presence of two competing factors, specifically the stiffening effect given by high modulus filler particles ($E = 70$ GPa for both silica [48] and GNP [49]) and the formation of aggregates because of the relatively poor dispersion within the matrix. Some studies reported the effect of β-phase content on the tensile properties and fracture behavior of isotactic PP [5]. In particular, it was shown how the elastic modulus and the yield stress decrease slowly with the β-phase content. Therefore, the nonmonotonical trend followed by the elastic modulus might also be attributed to crystals polymorphism. However, other effects should be accounted for, especially the dependence of morphology and filler interfacial interactions upon the filler content.

In addition, the impact strength values shown in Fig. 6 significantly increase with the filler content, with a greater enhancement in the case of GNP composites. Noteworthy, the increase in toughness obtained in PP composites at low and intermediate filler content can be ascribed to (i) changes in the energy absorbing mechanisms (i.e., higher plastic deformation of the matrix along the filler/matrix interface, crack branching due to hindrance by reinforcements, bridging of the crack, creation of voids, etc.) and (ii) different crystalline morphology occurring upon nanomodification. In particular, as already shown in the isothermal crystallization experiments, the presence of the filler may change the spherulite size. Moreover, the filler type and content can, as discussed earlier, affect the polymorphism and lamella thickness (see Isothermal Crystallization Behavior Section). Both spherulite size and polymorphism play a key-role in determining the impact strength of PP [2]. Some studies reported how an increase in β-phase content results in a significant enhancement in impact strength and toughness in PP [1, 13]. Since the investigated nanocomposites show a higher β-phase content at filler contents between 0.5 and 5 wt%, this might be one of the reasons explaining the higher impact strength observed with respect to unfilled PP, whose amount of β-phase is significantly lower.

CONCLUSIONS

The effect of silica and GNP nanoparticles on the crystallization behavior and polymorphism of isotactic PP was investigated by optical microscopy and XRD. Both silica and GNP were found to be effective nucleating agents, significantly increasing the crystallization rate during isothermal crystallization, with greater changes observed in case of GNP composites. PP crystals nucleate on the GNP surface, as observed in *in situ* crystallization studies using optical microscopy.

The nucleation of the β-phase, which manifests superior impact strength and toughness compared to the most common α-form crystals, was observed in both silica and graphite composites even at low filler concentration (as low as 0.01 wt%). A saturation effect on the nucleation and growth of the β crystals was observed at higher filler amounts (0.5 wt% for silica and

1 wt% for GNP) due to the relatively poor dispersion that limits the available filler surfaces for nucleation.

Because of the overall changes were found generally greater for GNP with respect to silica, the GNP is significantly more efficient in inducing polymorphism and favoring the formation of more perfect α-form crystals.

ACKNOWLEDGMENTS

The authors greatly acknowledge Dr. Mehdi Karevan and Dr. Md Bhuiyan—Woodruff School of Mechanical Engineering at Georgia Institute of Technology—for their kind assistance during the training for the use of machines and instruments.

REFERENCES

1. J. Karger-Kocsis, J. Varga, and G.W. Ehrenstein, *J. Appl. Polym. Sci*., **64**, 2057 (1997).
2. T.A. Huy, R. Adhikari, T. Lupke, S. Henning, and G.H. Michler, *J. Polym. Sci. B Polym. Phys*., **42**, 4478 (2004).
3. J. Karger-Kocsis, *Polypropylene: An A-Z Reference*, Kluwer Publishers, Dordrecht, The Netherlands (1999).
4. J. Karger-Kocsis, *Polym. Eng. Sci*., **36**, 203 (1996).
5. P. Tordjeman, C. Robert, G. Marin, and P. Gerard, *Eur. Phys. J. E*, **4**, 459 (2001).
6. H. Janeschitz-Kriegl, *Crystallization Modalities in Polymer Melt Processing*, Springer, Wien (2010).
7. J. Garbarczyk, D. Paukszta, and S. Borysiak, *J. Macromol. Sci. Phys*., **41**, 1267 (2002).
8. A. Menyhárd and J. Varga, *Eur. Polym. J*., **42**, 3257 (2006).
9. Y. Cao, J. Feng, and P. Wu, *J. Therm. Anal. Calorim*., **103**, 339 (2010).
10. A. Romankiewicz, T. Sterzynski, and W. Brostow, *Polym. Int*., **53**, 2086 (2004).
11. Z. Zhang, Y. Tao, Z. Yang, and K. Mai, *Eur. Polym. J*., **44**, 1955 (2008).
12. S.-Y. Park, Y.-H. Cho, and R.A. Vaia, *Macromolecules*, **38**, 1729 (2005).
13. J. Karger-Kocsis and J. Varga, *J. Appl. Polym. Sci*., **62**, 291 (1996).
14. W. Leelapornpisit, M.-T. Ton-That, F. Perrin-Sarazin, K.C. Cole, J. Denault, and B. Simard, J. *Polym. Sci*., *Part B: Polym. Phys*., **43**, 2445 (2005).
15. B.P. Grady, F. Pompeo, R.L. Shambaugh, and D.E. Resasco, *J. Phys. Chem. B*, **106**, 5852 (2002).
16. K. Kalaitzidou, H. Fukushima, P. Askeland, and L.T. Drzal, *J. Mater. Sci*., **43**, 2895 (2007).
17. D. Pedrazzoli, A. Dorigato, and A. Pegoretti, *J. Nanosci. Nanotechnol*., **12**, 4093 (2012).
18. J.A. King, M.D. Via, F.A. Morrison, K.R. Wiese, E.A. Beach, M.J. Cieslinski, and G.R. Bogucki, *J. Compos. Mater*., **46**, 1029 (2011).
19. K. Kalaitzidou, H. Fukushima, and L.T. Drzal, *Carbon*, **45**, 1446 (2007).
20. S. Kim, I. Do, and L.T. Drzal, *Macromol. Mater. Eng*., **294**, 196 (2009).
21. M. Tait, A. Pegoretti, A. Dorigato, and K. Kalaitzidou, *Carbon*, **49**, 4280 (2011).
22. L.T. Drzal and H. Fukushima, "Exfoliated Graphite Nanoplatelets (xGnP): A Carbon Nanotube Alternative," in *Technical Proceedings of the 2006 NSTI Nanotechnology Conference and Trade Show, Vol. 1, Boston (MA-USA), May 7–11 2006* (2006).
23. H. Kim, A.A. Abdala, and C.W. Macosko, *Macromolecules*, **43**, 6515 (2010).
24. R. Sengupta, M. Bhattacharya, S. Bandyopadhyay, and A.K. Bhowmick, *Prog. Polym. Sci*., **36**, 638 (2011).
25. H. Fukushima, *Graphite Nanoreinforcements in Polymer Nanocomposites*, Michigan State University, East Lansing, MI (2003).
26. E. James, *Polymer Data Handbook*, Oxford University Press, New York 1999.
27. W.A.Y. Yusoff, K.D. Dotchev, and D.T. Pham, *Proc. Inst. Mech. Eng. Part C: J. Mech. Eng. Sci*., **222**, 2163 (2008).
28. W. Zheng, X. Lu, C. Ling Toh, T. Hua Zheng, and C. He, J. *Polym. Sci*., *Part B: Polym. Phys*., **42**, 1810 (2004).
29. H. Dragaun, H. Hubeny, and H. Muschik, *Polym. Phys. Ed*., **15**, 1779 (1977).
30. A. Nogalesa, B.S. Hsiao, R.H. Somani, S. Srinivas, A.H. Tsou, F.J. Balta-Calleja, and T.A. Ezquerra, *Polymer*, **42**, 5247 (2001).
31. J.-H. Chen, F.-C. Tsai, Y.-H. Nien, and P.-H. Yeh, *Polymer*, **46**, 5680 (2005).
32. Q. Zheng, Y. Shangguan, S. Yan, Y. Song, M. Peng, and Q. Zhang, *Polymer*, **46**, 3163 (2005).
33. P. Supaphol and J.E. Spruiell, *J. Appl. Polym. Sci*., **75**, 337 (2000).
34. A. Turner Jones, J.M. AIizlewood, and D.R. Beckett, *Macromol. Chem. Phys*., **75**, 134 (1964).
35. E.W. Nuffield, *X-Ray* Diffraction Methods, Wiley, New York (1966).
36. D.D.L. Chung, *J. Mater. Sci*., **37**, 1475 (2002).
37. H. Mirzazadeh, A.A. Katbab, and A.N. Hrymak, *Polym. Adv. Technol*., **22**, 863 (2011).
38. E. Planes, J. Duchet, A. Maazouz, and J.-F. Gerard, *Polym. Eng. Sci*., **48**, 723 (2008).
39. T.G. Gopakumar and D.J.Y.S. Pagè, *Polym. Eng. Sci*., **44**, 1162 (2004).
40. K. Kalaitzidou, *Exfoliated Graphite Nanoplatelets as Reinforcement for Multifunctional Polypropylene Nanocomposites*, Ph.D. thesis, Michigan State University, East Lansing (MI-USA) 2006.
41. V. Petraccone, G. Guerra, C. De Rosa, and A. Tuzi, *Macromolecules*, **18**, 813 (1984).
42. C. Marco, M.A. Gomez, G. Ellis, and J.M. Arribas, *J. Appl. Polym. Sci*., **86**, 531 (2002).
43. J. Varga, *J. Therm. Anal*., **31**, 165 (1986).
44. J. Varga, G. Garzò, and A. Ille, *Angew. Makromol. Chem*., **142**, 171 (1986).
45. J. Varga and J. Karger-Kocsis, *J. Polym. Sci. Part B: Polym. Phys*., **34**, 657 (1996).
46. C. Passingham, P.J. Hendra, M.E.A. Cudby, V. Zichy, and M. Weller, *Eur. Polym. J*., **26**, 631 (1990).
47. B. Fillon, A. Thierry, J.C. Wittmann, and B. Lotz, *J. Polym. Sci. Part B: Polym. Phys*., **31**, 1407 (1993).
48. A. Dorigato, Y. Dzenis, and A. Pegoretti, *Mech. Mater*., **61**, 79 (2013).
49. M. Karevan, R.V. Pucha, M.A. Bhuiyan, and K. Kalaitzidou, *Carbon Lett*., **11**, 325 (2011).